The evolution of mode-2 internal solitary waves modulated by background shear currents

Peiwen Zhang [1, 3], Zhenhua Xu [1, 2*], Qun Li [4*], Baoshu Yin [1, 2, 3], Yijun Hou[1, 2, 3], Antony K. Liu[5]

5 [1]Key Laboratory of Ocean Circulation and Waves, Institute of Oceanology, Chinese Academy of Sciences, Qingdao, 266071, China.

[2]Qingdao National Laboratory for Marine Science and Technology, Qingdao, 266071, China.

[3]University of the Chinese Academy of Sciences, Beijing, 100049, China.

[4]Polar Research Institute of China, Shanghai, 200136, China.

10 [5]Ocean University of China, Qingdao, 266100, China.

Correspondence to: Zhenhua Xu (xuzhenhua@qdio.ac.cn)

Abstract. The evolution process of mode-2 internal solitary waves (ISWs) modulated by the background shear currents was investigated numerically. The forward-propagating long wave, amplitude-modulated wave packet were generated during the early stage of modulation, where the

15 amplitude-modulated wave packet were suggested playing an important role in the energy transfer process, and then the oscillating tail was generated and followed the solitary wave. Five different cases were introduced to assess the sensitivity of the energy transfer process to the Δ, which defined as a dimensionless distance between the centers of pycnocline and shear current. The forward-propagating long waves were found robust to the Δ, but the oscillating tail and amplitude-modulated wave packet

20 decreased in amplitude with increasing Δ. The highest energy loss rate was observed when $\Delta = 0$. In the first 30 periods, ~36% of the total energy lost at an average rate of 9 W m^{-1}, it would deplete the energy of the solitary wave in ~4.5 h, corresponding to a propagation distance of ~5 km, which is consistent with the hypothesis of *Shroyer et al*. (2010), who speculated that the mode-2 ISWs are "short-lived" in the presence of shear currents.

1 Introduction

25 Internal solitary waves (ISWs) are commonly observed in stratified oceans, especially in coastal and continental shelf regions (Grimshaw et al., 2010;Helfrich and Melville, 2006; Lamb, 2014). While mode-1 ISWs are frequently observed by in situ observations (Farmer et al., 2009; Klymak and Moum,

2003; Moum et al., 2006) and by remote sensing (Liu et al., 1998; Liu et al., 2004; Zhao et al., 2004; Zhao and Alford, 2006), higher modes are relatively rare captured. Even so, with the improvement of observation, mode-2 ISWs have been reported recently (Liu et al., 2013; Shroyer et al., 2010; Yang et al., 2009; Yang et al., 2010). Most of previously reported mode-2 ISWs were categorized as convex types, which have the potential to transport mass (Brandt and Shipley, 2014; Deepwell and Stastna, 2016; Salloum et al., 2012). In contrast, concave mode-2 ISWs are not as frequently observed in slope areas as convex types. Yang et al. (2010) suggested that the occurrence of concave mode-2 ISWs requires the presence of a thick pycnocline, which is rarely present in a shallow sea.

Majority of studies of mode-2 ISWs aimed at interpreting their generation mechanisms under different conditions (Helfrich and Melville, 1986; Huttemann and Hutter, 2001; Stastna and Peltier, 2005; Vlasenko et al., 2010). Yuan et al. (2018) investigated the propagation of mode-2 ISWs over slope-shelf topography, suggesting the propagation manner of mode-2 ISWs over a slope is similar to the mode-1 ISW, but presenting a rather complex wave field. Under most circumstances, mode-2 ISWs show the specific phenomenon of a "short-lived" nature (Ramp et al., 2012; Shroyer et al., 2010; Yang et al., 2010). Ramp et al. (2012) concluded that mode-2 ISWs around the Heng-Chun Ridge would dissipate in 8.9 hours, suggesting mode-2 ISWs are highly dissipative when traveling around rough topographical features. Stastna et al. (2015) investigated the strong interaction between mode-1 and mode-2 ISWs, illustrating the mode-2 ISWs deformed significantly and became ephemeral during the interaction. Terletska et al. (2016) showed the decaying of mode-2 ISWs was induced by a step-like topography. The forward-propagating long waves, breather-like internal waves (BLIWs) and an oscillating tail were generated during the adjustment process.

The ephemeral phenomenon of mode-2 ISWs could also be induced by the background shear currents. They are more common in the open ocean because they can be induced by the baroclinic eddies, baroclinic tides, wind and internal solitary wave (Chen et al., 2011; Wang et al., 1991; Xu et al., 2013; Xu et al., 2016). In cases with large-scale currents, such as those induced by the wind and internal tides, the background currents should be present before the generation of the mode 2 ISW. Additionally, this circumstance is also possible in the presence of small-scale background currents and was observed by Orr and Evans (2015) over the New Jersey Shelf, which is near the field site of Shroyer et al. (2010). The steepening of internal tides generates both mode-1 and mode-2 ISWs on the New Jersey Shelf, and the mode-1 wave, which has a faster propagation speed, can overtake the mode-2 wave generated in the

last period of the internal tide (Orr and Evans, 2015).

Previous works focused on the shoaling pycnocline and topography, which were suggested to cause the ephemeral mode-2 ISWs, but the effects of background shear currents were neglected (Shroyer et al., 2010). Given the background conditions described by Shroyer et al. (2010), the stratification remains

5 stable with a flat bottom, but the presence of background shear current could modulate the mode-2 ISW. Therefore, the authors speculated that the background shear currents could produce instabilities and lead to the adjustment of ISWs. Motivated by the hypothesis of Shroyer et al. (2010), in the present study, we investigated the influence of shear currents on the mode-2 ISWs and presented the evolution processes and energy of mode-2 ISWs using numerical simulations. Five different cases were

10 introduced to investigate the propagation of mode-2 ISWs in the presence of shear currents, since the background shear currents could symmetric around the center of the pycnocline or deviate for a distance from it. These conditions are common in the oceans, for example, the internal tidal wave could be symmetric around the pycnocline, but in the shelf-slope area, the surface-intensified flow driven by wind could deviate for a distance from the center of pycnocline.

15 The paper is organized as follows: The numerical model configurations and background conditions are detailed in Sect. 2. In Sect. 3, the results are presented and examined. The energy transfer process and the decaying of the mode-2 ISWs are analyzed in Sect. 4. In Sect. 5, details of mode-2 ISW evolution are discussed and compared. Then, the results are summarized in Sect. 6.

2 Numerical model and background condition

2.1 Model configuration

Our numerical simulations are based on the Massachusetts Institute of Technology general circulation

20 model (MITgcm, Marshall et al., 1997). The nonhydrostatic capability of the MITgcm is turned on because ISWs represent a balance of nonlinearities and dispersions, with the latter derived from nonhydrostatic pressure. The MITgcm integrates the incompressible Boussinesq equations, and a linear equation of state was used in these simulations with an implicit free surface. (See the documentation of the MITgcm, http://mitgcm.org, for more details.)

25 A series of 2D numerical simulations were performed to investigate the evolution of mode-2 ISWs in the presence of background shear currents. The experimental domain was 12.8 km long and 100 m

deep. The horizontal and vertical resolutions were 2.5 m with 5120 grids points and 0.5 m with 200

grid points, respectively. The time step was 0.4s in order to ensure that the Courant-Friedrichs-Lewy

(CFL) condition was satisfied and the model was stable. The viscosity parameters were set to 10^{-3}

m²s⁻¹ for v_H and 10^{-4} m² s⁻¹ for v_v in the present study. The flux-limiting advection scheme for the

5   tracers introduces numerical diffusivity which is needed for stability, so the explicit diffusivity was set

to zero (Legg and Adcroft, 2003, Legg and Huijts, 2006, Legg and Klymak, 2008).

2.2 Stratification and background conditions

The choice of background density stratification and shear currents followed the field observations over

the New Jersey shelf (Shroyer et al., 2010). The background stratification and shear currents adopted

the hyperbolic tangent function for smoothing, which can be written as follows:

10    $$\rho(z) = \rho_0 - \frac{\Delta\rho}{2}tanh\left[\frac{(z+z_0)}{h}\right],$$ (1)

where $\rho_0 \equiv (\rho_1 + \rho_2)/2$ is the mean density of the vertical water column and $\Delta\rho \equiv (\rho_2 - \rho_1)$ is the

difference in density between the upper layer ρ_1 and bottom layer ρ_2. The h is the pycnocline

thickness and z_0 is the depth of the pycnocline center. The function of background shear current is

given by

15    $$U(z) = U_0 - \frac{\Delta U}{2}tanh\left[\frac{(z+D_s)}{h_s}\right],$$ (2)

where $U_0 \equiv (U_1 + U_2)/2$ is the mean background velocity of water column and $\Delta U \equiv (U_2 - U_1)$ is

the difference in background horizontal velocity between the upper layer U_1 and bottom layer U_2, and

h_s is the thickness of shear layer. To reveal the sensitivity of energy transfer process to the relative

locations of the pycnocline and background shear current, we introduced a dimensionless value Δ,

20   which was defined as the distance between the centers of pycnocline and shear current

nondimensionalized by the $h/2$, and the D_s indicates the center depths of the shear currents for five

cases with different Δ. The vertical distributions of the background shear currents, density and

buoyancy frequency are shown in Fig. 1, and the detailed values for background stratification and

currents in the present study are given in Table 1. In all five cases, the Richardson number were

25   estimated to be larger than 0.25, indicating the stable state of the background environment (Fig. 2).
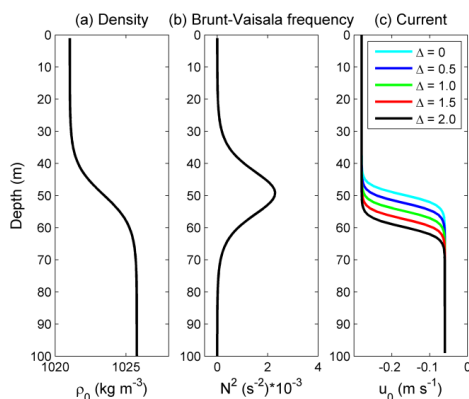
Figure 1: Vertical profiles of the (a) density, (b) buoyancy frequency and (c) background velocities in the simulations, which includes the $\Delta = 0$ (case 1), $\Delta = 0.5$ (case 2), $\Delta = 1.0$ (case 3), $\Delta = 1.5$ (case 4) and $\Delta = 2.0$ (case 5) marked by the cyan, blue, green, red, and black lines, respectively.

5 **Table 1:** The parameter values for the initial background conditions

Parameters	Values
ρ_1	1026 kg m^{-3}
ρ_2	1022 kg m^{-3}
h	10 m
z_0	50 m
U_1	-0.28 m s^{-1}
U_2	-0.06 m s^{-1}
h_s	3 m
D_s ($\Delta = 0, 0.5, 1.0, 1.5, 2.0$)	50, 52.5, 55, 57.5, and 60 m
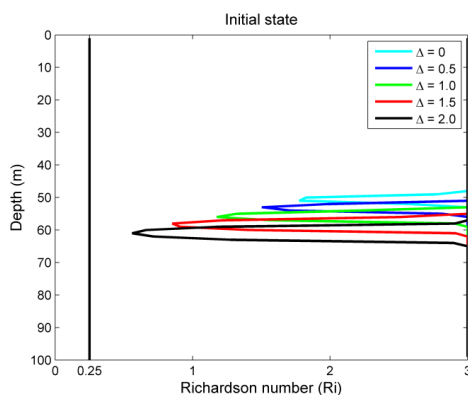
Figure 2: Richardson numbers of the background state for the five cases with the Δ = 0, 0.5, 1.0, 1.5 and 2.0 marked by the cyan, blue, green, red, and black lines, respectively.

2.3 Modal initialization

Rank-ordered mode-2 ISW train was generated by the "lock-release" method (Brandt and Shipley,

5   2014;Helfrich et al., 2010; Sutherland et al., 2013). Figure 3 demonstrates the configurations of the simulation domains. A mixed region was set symmetric around the centerline of the pycnocline at the right end, with a length of 375 m and height of 25 m. The pycnocline was 10 m thick, and this dimension was indicated by h. the model was initialized at t = 0 s, and the rank-ordered mode-2 wave train emerged at t = 4000 s and propagated to the left of the domain, as shown in Fig. 3, the leading

10   mode-2 wave is extracted at that time and then propagated for 2000 s until it stabilized. A is the amplitude of mode-2 ISW, and the wavelength L was defined as the width of the wave at half the amplitude. At 6000 s after the initialization of numerical model, the background shear currents were initialized in experiment.
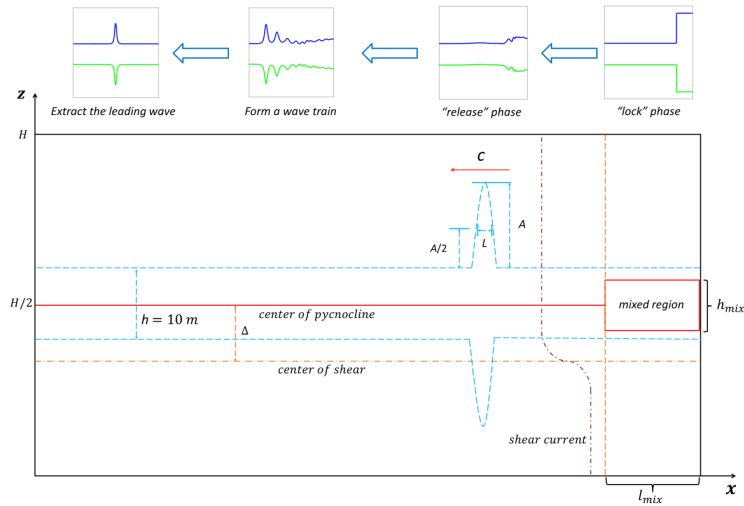
Figure 3: Schematic diagram of the modal configuration and initialization.

3 Results

3.1 Characteristics of mode-2 ISWs

The vorticity and temperature fields of the leading single wave of a mode 2 ISW in the absence of the background shear current are shown in Fig. 4. The ISW had amplitude of 7 m, wave length of 62.5 m

5 with a propagation speed at ~0.31 m s^{-1}, which was defined as c. It is slightly larger than the linear long-wave phase speed c_p calculated by the Taylor-Goldstein equation (Vlasenko et al., 2010). The typical time scale T for mode-2 ISW is 200 s which was calculated by L/c, and the wave exhibits a notably symmetric structure without mode-1 wave tail. As such, the mode-2 ISW remains stable and has the potential to propagate over a long distance. This finding is confirmed by the vorticity field

10 shown in Fig. 4(b), which shows a stable and symmetric vortex dipole.
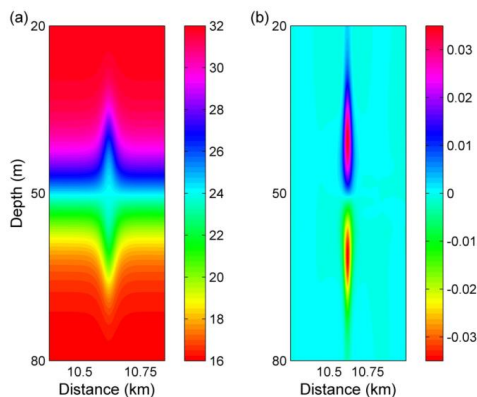
Figure 4: The characteristics of a single mode-2 ISW's (a) wave form and (b) vorticity in the absence of background shear current.

3.2 The evolution of mode-2 ISW in case 1

The evolution of a mode-2 ISW modulated by the background shear current in case 1 ($\Delta = 0$) is shown

5   in Fig. 5, with its corresponding vorticity field shown in Fig. 6. The mode-2 ISW was symmetric about the pycnocline center and the vorticity of the upper and lower parts counterbalance each other in the initial state (Fig. 5 (a) and Fig. 6 (a)).
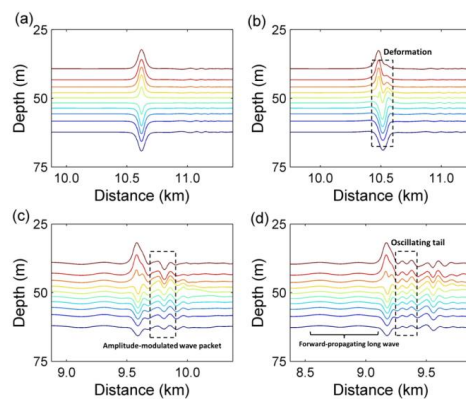
Figure 5: The evolution process of the mode-2 ISW in the case 1 ($\Delta = 0$) for the different times (a) 0T, (b) 1.2T, (c)
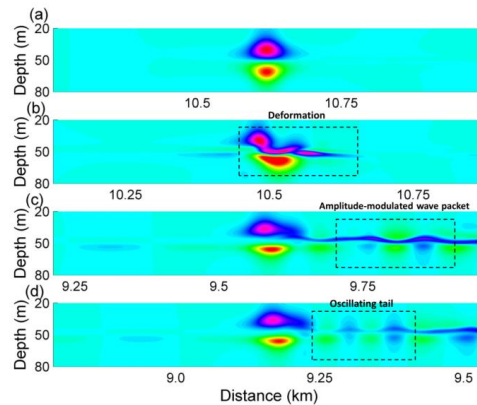
10   10T, (d) 14T.

Figure 6: The evolutiona process of the vorticity field in the case 1 ($\Delta = 0$)for the different times (a) 0T, (b)1.2T, (c) 10T, (d) 14T.

Then, at 1.2 T after the initialization of background shear current, as shown in Fig. 6 (b), the shear led

5   to the deformation of the dipole, with the upper part being pushed forward. It also caused the asymmetrical distribution of the vorticity in horizontal, which is associated with the generation of forward-propagating long waves and amplitude-modulated wave packet (Fig. 5 (b)). In the aft of the ISW, The shear induced by the background currents lead to the deformation of the vortex dipole, and an increasing complexity of the vorticity field implied more energy is transferred from mode-2 ISWs to

10   other wave forms. As illustrated in Fig. 6 (c), 10 T after the initialization of background shear current, the vorticity of the mode-2 ISW is redistributed to adapt to the background condition. In that process, which is related to the generation of an amplitude-modulated wave packet and a forward-propagating long wave, some of the energy of the ISW was transferred to them, and consequently, the vortex of the ISW shrank. The forward-propagating long wave and amplitude-modulated wave packet can be seen in

15   Fig. 5 (c), with amplitudes of 0.25 m and 1.8 m respectively, implying the amplitude-modulated wave packet is more energetic.

The oscillating tail caused by the shear was visible between the mode-2 ISW and amplitude-modulated wave packet (Fig. 5 (d)) at 14 T after the initialization of background shear current. The amplitude-modulated wave packet propagated independently from the ISW, indicating that they were

20   no longer related to the energy transfer of the mode-2 ISW. Based on the vorticity field shown in Fig. 6 (d), the generation of the oscillating tail and the forward-propagating long wave was continuously sustained by the energy of the ISW. Therefore, they have the potential to drain the energy from an ISW

over a long time scale. It should be noted that the forward-propagating long wave formed when the background shear current is present. Thus, the energy loss of the ISW caused by forward-propagating long waves occurs earlier than oscillating tail.

3.3 The evolution of mode-2 ISW in case 5

In other cases (Δ = 0.5, 1.0, 1.5, 2), the shear current was set to deviate from the pycnocline center to

5 examine the influence of the relative distance on the energy transfer process of mode-2 ISWs. The case 5 (Δ = 2) was examined in the following section. The evolution of the mode-2 ISW in the case 5 and its corresponding vorticity field are shown in Fig. 7 and Fig. 8, respectively.
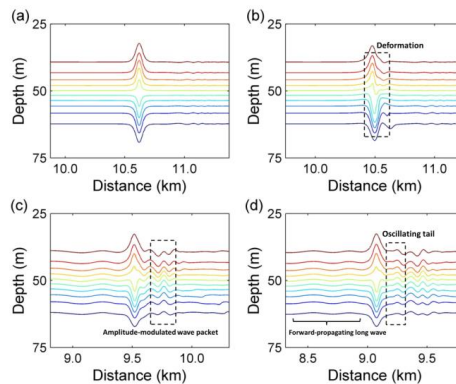
Figure 7: The evolution processes of the mode-2 ISW in the case 5 (Δ = 2.0) at different times (a) 0T, (b) 1.2T, (c)
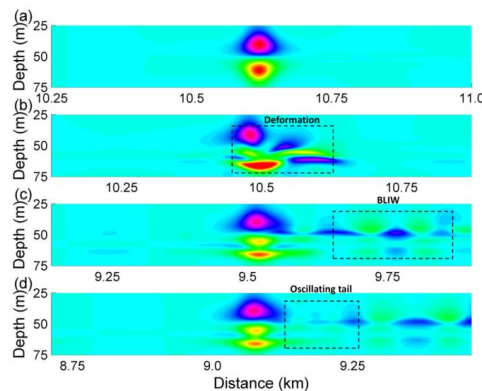
10 10T, (d) 14T.

Figure 8: The evolution process of the vorticity field in the case 5 (Δ = 2.0) for different times of (a) 0T, (b)1.2T,

(c) 10T, (d) 14T.

The deformation of the vortex dipole at 1.2 T after the initialization of background shear current is illustrated in Fig. 8 (b). The shear vertically distorted the lower section of the vortex and forced some of the vortices from the lower part of the dipole to penetrate the upper part. Redistribution of vorticity occurred both vertically and horizontally. The upper section was bifurcated such that the branch

5   containing most of the vorticity intruded ahead, which related to the generation of a forward-propagating long wave in the same manners at that in the case 1, as shown in Fig. 7 (b). The other branch moved backward to the aft of the ISW, corresponding to the generation of amplitude-modulated wave packet. Given this modulation process, while the lower part of the dipole obviously shrank, the upper parts slowly reunited to restore the vertical balance.

10   The vorticity distribution was different from that of the case 1 at 10 T after the initialization of background shear current (Fig. 8 (c)). The lower part of the vortex had two obvious cores, which were separated by the shear effect and jointly balanced with the upper section. The amplitude-modulated wave packet and forward-propagating long waves are plotted (Fig. 7 (c)). The amplitude of the wave packet was 1 m, which was smaller than that of the case 1, suggesting that the energy transfer process

15   was weakened. However, the amplitude of the forward-propagating long wave was still approximately 0.25 m, implying that the forward-propagating long wave may not be affected by the Δ. In Fig. 7 (d), an oscillating tail with 0.25 m amplitude developed at the rear of the wave. It was sustained by the energy transferred from the ISW, as shown in Fig. 8 (d). The small amplitude of the oscillating tail and amplitude-modulated wave packet indicate that the energy loss caused by the shear was weaker in the

20   case 5 than in the case 1, but the weakening of the oscillating tail makes the amplitude-modulated wave packet more visible.

3.4 The relationship between the energy transfer process and Δ

The amplitude of the different types of waves which were shed from the mode-2 ISWs in five cases are given in Fig. 9 , to reveal the effects of the Δ on the modulation of the mode-2 ISW. Through a comparison of different cases from $\Delta = 0$ (case 1) to $\Delta = 2$ (case 5), the modulation caused by

25   background shear currents have been weakened as the Δ increased, corresponding to the decreased amplitude of the amplitude-modulated wave packet and oscillating tail. The amplitude of wave-packet decreased from 1.8 m to 1 m monotonically, and the amplitudes of the oscillating tails decreased from 0.85 m to 0.25 m between the case 1 ($\Delta = 0$) and the case 3 ($\Delta = 1$), but remained stable between the

case 3 ($\Delta = 1$) and case 5 ($\Delta = 2$), indicating that the amplitude-modulated wave packet were more sensitive to the Δ than the oscillating tail. As the Δ increased, the modulation caused by the background shear current decreased, further causing weakened energy transfer process and shrinking the amplitude. As expected, the ratio between the amplitude of modulated wave packet and oscillating tails increased

5   from 2.1 in the case 1 to 4 in the case 5, so the amplitude-modulated wave packet became more distinct in case 5. The amplitude-modulated wave packet has the highest amplitude among all cases compared to those of the other two wave forms. Thus, amplitude-modulated wave packet could play an important role of energy transfer in the initial stages of the modulation processes. In contrast, the forward-propagating long wave barely affected by Δ and remained constant at approximately 0.25 m in

10   all cases. This divergence of sensitivity between the forward-propagating long wave, amplitude-modulated wave packet and oscillating tail could be related to their generation mechanisms, which needs further study.
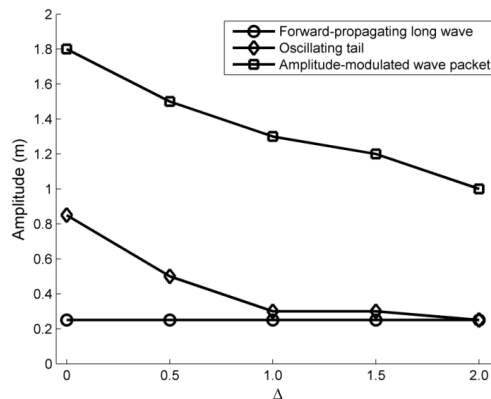
Figure 9: The amplitude of the different types of waves which were shed from the mode-2 ISWs in five cases are

15   shown; circles represent the forward-propagating long wave, diamonds represent the oscillating tail and squares represent the amplitude-modulated wave packets.

4 Energy analyses

4.1 Calculation of energy

The evolution of the mode-2 ISWs in the presence of shear currents was analyzed quantitatively in terms of energy. The available potential energy (APE) and kinetic energy (KE) of the dissipations were calculated. The equations are

$$KE = \int_{x_l}^{x_r} \int_{-H(x)}^{0} \rho_0 (u^2 + w^2) dx dz, \qquad (3)$$

$$APE = \int_{x_l}^{x_r} \int_{-H(x)}^{0} (\rho - \bar{\rho}) gz dx dz,$$

(4)

And the total energy E is written as:

5    $E = KE + APE,$

(5)

where $\bar{\rho}$ is the reference density extracted from the initial field, ρ_0 is the averaged density and ρ is the fluid density. x_r and x_l are the boundaries location of the integration region, and the x satisfied $x_l \leq x \leq x_r$. The u and w are the horizontal and vertical velocity induced by the wave, respectively, and

10   they were extracted without the background velocity. The total energy of the initial mode-2 ISW calculated by the above expressions was 146.2KJ m^{-1}.

Using the method introduced by Lamb and Nguyen (2009), we set two transects at the front and rear edges of the mode-2 ISW to compute the energy fluxes radiating from the ISW. The total energy flux through a transect is:

15    $E_f = KE_f + APE_f + W,$

(6)

where KE_f, APE_f and W are the kinetic, available potential and pressure perturbation energy fluxes, respectively. They are written as:

$$KE_f = \int_{-H(x)}^{0} uKE dz, \qquad (7)$$

20    $$APE_f = \int_{-H(x)}^{0} uAPE dz, \qquad (8)$$

$$W = \int_{-H(x)}^{0} up_d dz, \qquad (9)$$

where u is the horizontal velocity induced by the mode-2 ISWs, and p_d is the pressure perturbation relative to the reference state (Lamb and Nguyen, 2009).

4.2 The cascading process of energy

The EOF method was applied to the modal decomposition according to Venayagamoorthy and Fringer

25   (2007), since the standard normal modes method is not suitable for the analysis of nonlinear and nonhydrostatic forward-propagating long wave, amplitude-modulated wave packet and oscillating tail.

Because of the shear effect on the mode-2 ISWs, the energy can cascade into all the modes, including mode-1 and higher modes. The vertical and horizontal kinetic energy modal distributions of different wave forms shed from the mode-2 ISW in the case 1 are shown in Fig. 10. In the forward-propagating long waves, the kinetic energy was all in the mode-1 form because of its propagation in front of the

5   ISWs, indicating the generation of the forward-propagating long waves corresponds to a cascading process from higher to lower modes. Figure.10 shows that the energy was mainly mode-1 in the oscillating tail and the amplitude-modulated wave packet, but weak mode-2 signals were also present, which was expected since the oscillating tail and amplitude-modulated wave packet follow the mode-2 ISW. The presence of mode-2 energy for the oscillating tail and amplitude-modulated wave packet is

10 reasonable because they have shorter wavelengths and slower phase speeds than the mode-2 ISW and propagate following the mode-2 ISW (Akylas and Grimshaw, 1992; Vlasenko et al., 2010).
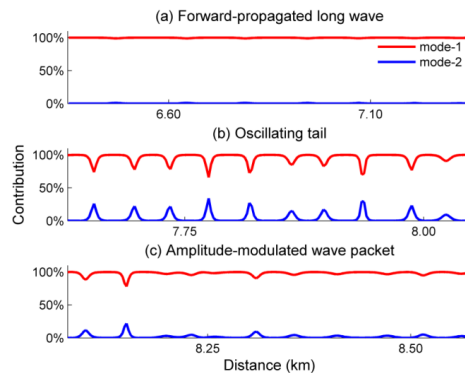
Figure 10: Percent contributions of mode-1 and mode-2 to the total kinetic energy in case 1 ($\Delta = 0$) at 30 T for the (a) forward-propagating long wave, (b) oscillating tail and (c) amplitude-modulated wave packet.

4.3 Energy loss of mode-2 ISW

15 In the case 1, ~36% of the total energy of the mode-2 ISW was lost by 30 T, part of that energy was transferred to other wave forms. During the first 30 T, The average energy loss rate was 9 W/m, such that all of the energy of the mode-2 ISW would be drained in 4.5 h, or by approximately 82 T, as we defined above, with a propagation distance of ~5 km. Modulated by the background shear current, the mode-2 ISW exhibits a "short-lived" nature and high energy loss rate, which is comparable to that of

20 the longer mode-1 ISW (Lamb and Farmer, 2011; Shroyer et al., 2010).
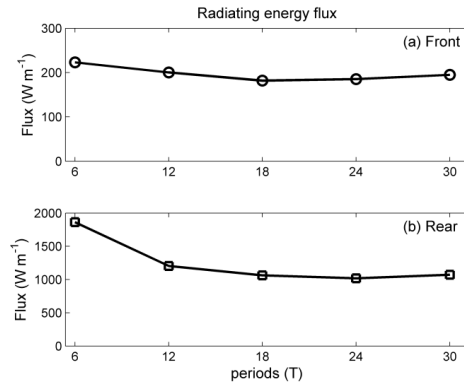
Figure 11: Vertical integrals of the radiating energy flux in the (a) front and (b) rear transects of the mode-2 ISW

in case 1 (Δ = 0) at different times.

For the case 1, we calculated the radiating energy flux (Fig. 11) to investigate the detailed energy

5   transport. The radiating energy flux in the front transect was nearly constant at approximately 0.2 KW

m^{-1}, indicating the forward-propagating long wave drains the energy of the mode-2 ISW at a constant

rate in the presence of a background shear current. In the rear transect, the radiating energy flux

decreased from 1.8 KW m^{-1} to 1.2 KW m^{-1} before stabilizing at approximately 1.0 KW m^{-1} above 12 T.

The energy flux at the crest of the amplitude-modulated wave packet and the oscillating tail ranged

10   from 1.0 KW m^{-1} to 2.5 KW m^{-1} and 0.3 KW m^{-1} to 1.1 KW m^{-1}, respectively. Combining with the

evolution process, the high radiating flux before 12 T indicates the generation process of the

amplitude-modulated wave packet and that the relative low radiating energy flux above 12 T is caused

by the generation of an oscillating tail.
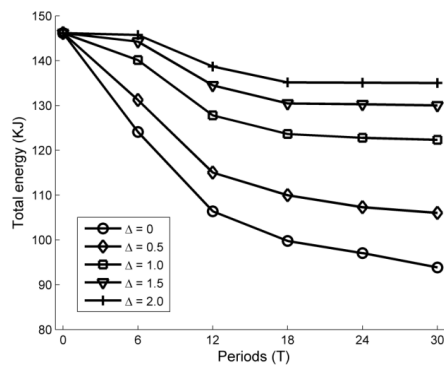
15   **Figure 12:** The total energy of the ISW in the different times and cases; circles represent the case 1 (Δ = 0),

diamonds represent the case 2 (Δ = 0.5), squares represent the case 3 (Δ = 1.0), triangles represent the case 4 (Δ =

1.5) and crosses represent the case 5 (Δ = 2.0).

The total energy of the mode-2 ISWs in the different cases and times are shown in Fig. 12, and the averaged energy loss rates at each period are given in Table 2. From 0 to 6 T, the averaged energy loss rates decreased significantly, from 18.4 W m^{-1} (case 1) to 0.4 W m^{-1} (case 5). This period corresponded

5   to the generation of the amplitude-modulated wave packet and forward-propagating waves, during which a deformation was caused by the shear to the aft of the ISW. The averaged energy loss rates from 6 to 12 T, decreasing as the Δ increased. This stage contained the exit of the amplitude-modulated wave packet, which occurred at approximately 10 T (Fig. 5 and Fig. 7), and the generation of the oscillating tail. In the case 1, ~34% of the total energy loss (52.34KJ m^{-1}) lost at an average rate of 14.8 W m^{-1}

10   from 6 to 12 T, and some of the energy transferred to the amplitude-modulated wave packet. High energy loss rate shown in Table 2 could be explained by this transfer process. Thus, in the early stage of modulation, the amplitude-modulated wave packet was suggested occupying an important role of energy transfer process. After the amplitude-modulated wave packet shed from the mode-2 ISWs, sharply decreased loss rates could be seen in 12 – 18 T, during which the energy loss was caused by the

15   forward-propagating long waves and the oscillating tail. The shear currents continuously sustained the development of the oscillating tail and the forward-propagating long waves. Thus, these two forms could slowly drain the energy of the ISW, with an average rate of 3.5 W m^{-1} in the case 1. In the following periods, with the nearly constant forward-propagating long waves and oscillating tails, the ISWs decayed with a relatively low rate. This was reinforced by a similar result given by Olsthroon et

20   al. (2013).。

Table 2: The energy loss rates (W m^{-1}) of the ISWs in different cases at different times.

	0 - 6 T	6 T – 12 T	12 T – 18 T	18 T – 24 T	24 T – 30 T
Case 1 (Δ = 0)	18.4	14.8	5.6	2.3	2.7
Case 2 (Δ = 0.5)	12.5	13.5	4.2	2.3	1.1
Case 3 (Δ = 1.0)	5.1	10.3	3.5	0.8	0.37
Case 4 (Δ = 1.5)	1.7	8.2	3.4	0.2	0.15
Case 5 (Δ = 2.0)	0.4	5.9	3.0	0.05	0.06

The energy loss rate of the case 1 was obviously higher than that of other cases, since the amplitude of

those mode-1 waves was largest among the cases. The energy loss decreased as the Δ increased, which corresponded to monotonic decrease of the amplitudes of different mode-1 wave forms. After 12 T, the energy loss rates in the different cases became smaller, since the oscillating tail and forward-propagating long waves with a relatively low energy transfer rate lead to the energy loss of

5   mode-2 ISW. Hence, the strength of energy loss of mode-2 ISW can be predicted by the Δ at the early stage of modulation.

5 Discussions

In the simulations of the present study, the wavelengths and amplitudes of mode-2 ISWs were selected to be comparable to the observations. Among those cases, the case 2 correspond to the observation by Shroyer et al. (2010) since the center of shear current was displaced by a similar distance from the

10   pycnocline center. A depression wave at the rear of the ISW in the first transect of wave *Jasmine* was similar to the wave form around 10 T in the numerical simulation (Fig. 3 (a) in Shroyer et al., 2010). Thus the first, second and third transects of wave Jasmine corresponded to 10 T, 23 T and 38 T in the case 2, respectively. The energy loss rates in 10 T and 23 T were 13.5 W m^{-1} and 2.3 W m^{-1}, the averaged energy loss rate between 10 T and 38 T was 5.1 W m^{-1}, they were in same scale with the

15   corresponding observations. Between 10 T and 38 T, ~20% of mode-2 ISW total energy lost,it was a little smaller than the typical observation results. Relatively high energy loss rate and a large amplitude oscillating tail in the third transect of the field observations could be probably attributed to the effect of a shoaling pycnocline (Shroyer et al., 2010) and thus the enhancement of the asymmetries in stratification, which could increase the energy loss of the wave during the propagation of mode-2 ISWs

20   (Carr et al., 2015; Olsthoorn et al., 2013).

The superposition of an initially stable shear current and the mode-2 ISW induced low Ri region with a minimum value of less than 0.01, suggesting the possible development of shear instability. The ISW tends to adjust gradually and adapt to the new background conditions. The vorticity and Ri of adjustment process for the mode-2 ISW in the case 1 is shown in Fig. 13. The Ri values are larger than

25   0.25 before 0.8 T. After 0.8 T, due to the shear currents and weakened stratification, the lowest Ri values decrease below 0.01 and are accompanied by increased vorticity around the low Ri region, indicating the generation of shear instability (Pawlak and Armi, 1998). Then, the Ri values increased

larger than 0.25, and the stratification is restored above 6.8 T. For the case 5 (Fig. 14), before 0.8 T, the Ri values are also larger than 0.25. They decrease below 0.01 near the depths of the shear current after 0.8 T, which is accompanied by the increased vorticity and weakened stratification, indicating the occurrence of the shear instability. The stratification is restored and the Ri values increased larger than

5   0.25 after 2 T. Compared to the case 1, the region with low Ri and increased vorticity was smaller in the case 5, making the instability process was less apparent, and the shear instability for the case 1 occurs at the same time but lasts longer than that for the case 5. Those comparison illustrated the adjustment of mode-2 ISWs modulated by the shear current are more energetic with small Δ, it is consistent with the results that the case 1 has the largest energy loss rate among all cases.
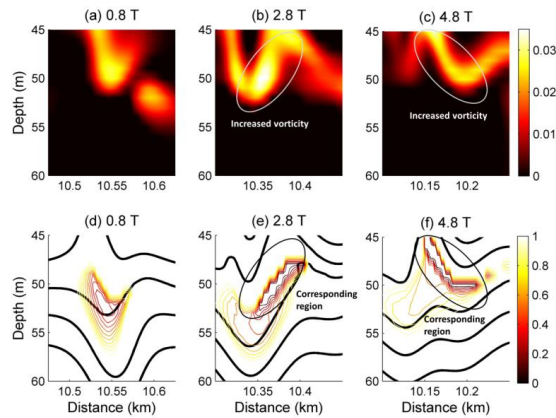
Figure 13: The vorticity spatial distributions for the case 1 (Δ = 0) at (a) 0.8 T, (b) 2.8 T, (c) and 4.8 T, and the corresponding Ri values at (d) 0.8 T, (e) 2.8 T, and (f) 4.8 T.
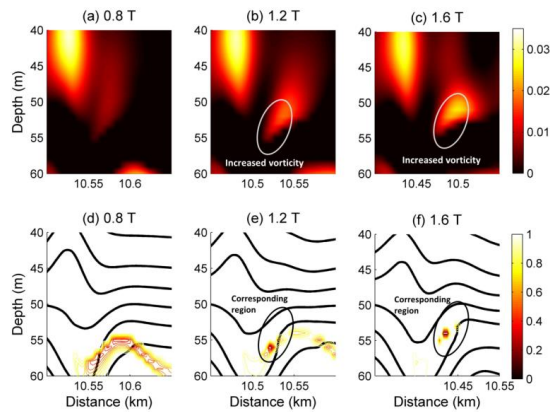
Figure 14: The vorticity spatial distributions for the case 5 (Δ = 2) at 0.8 T (a), 1.2 T (b), and 1.6 T (c), and the

corresponding Ri values at 0.8 T (d), 1.2 T (e), and 1.6 T (f).

In our simulations, the modulation of mode-2 ISW in the presence of shear currents excites the amplitude-modulated wave packet, whose characteristics are similar to a breather-like internal wave (Terletska et al., 2016). Internal breather waves are periodically pulsating, isolated wave forms, they are

5   also a type of steady state wave solution of the extended Korteweg-de Vries equation (Lamb et al., 2007), and has been found to exist in the real ocean (Vlasenko and Stashchuk, 2015). We introduced the definition of breather by Clarke et al. (2000) to clarify the characteristics of amplitude-modulated wave packet. The envelop lines of the amplitude-modulated wave packet in case 1 are shown in Fig. 15. Inside the envelop lines, the oscillatory pulses freely oscillate, satisfying the breather definition.

10   Additionally, the energy inside the envelope was calculated and remains nearly constant from 12 to 28 T. Similar to the case 1, the characteristics and energy loss of the amplitude-modulated wave packet for the case 5 were also similar with the breather definition. Noted that the breather solution exist only if the cubic nonlinearity coefficients in Gardner equation is positive (Lamb et al., 2007), but the configuration of the stratification in our simulation results a negative cubic nonlinearity coefficient in

15   Gardner equation (Grimshaw et al., 2010; Talipova et al., 2011) and it means the breather is not allowed in this stratification. Similar results were revealed by Terletska et al. (2016), the interaction of mode-2 internal waves with a step-like topography could induce the generation of BLIWs (breather-like internal waves), providing a possibility of the breather generation in a thin intermediate layer with a range of intermediate wavelength.
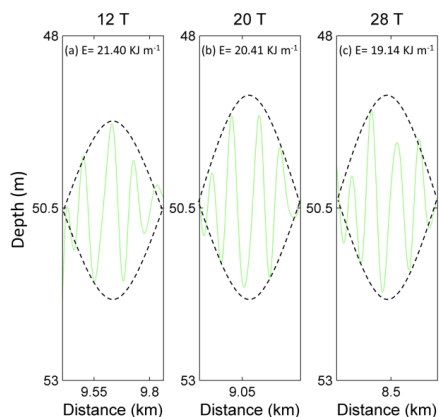
Figure 15: The envelopes of the amplitude-modulated wave packet in the case 1 ($\Delta = 0$) at (a) 12 T, (b) 20 T and (c) 28 T.

The oscillating tail was frequently observed in similar studies (Carr et al., 2015; Olsthoorn et al., 2013; Stastna et al., 2015). Its generation was related to the shear, and the tail was sustained by continuous energy input. The presence of the background shear current modulated the mode-2 ISW and induced the continuously energy transfer process from the main wave to the oscillating tail, supporting its existence. Forward-propagating long waves were also observed in Terletska et al. (2016). A forward-propagating long wave with nearly constant amplitude could drain the energy of mode-2 ISWs at a steady rate, and then leads to an inevitable energy loss of those mode-2 ISWs in the presence of background shear.

The numerical simulation results shown above indicate the amplitude-modulated wave packet, oscillating tails and forward-propagating long waves were generated during the adjustment of the mode-2 ISWs in the presence of the shear currents. Those wave forms are common in the adjustment of mode-2 ISWs (Carr et al., 2015; Olsthoorn et al., 2013; Terletska et al., 2016), but the generation mechanism of amplitude-modulated wave packet requires further examination.

6 Conclusions

We have presented the evolution process of mode-2 ISWs modulated by the background shear current with the MITgcm in this study. We illustrated the adjustment of the mode-2 ISWs in the presence of background shear current occurs through the generation of forward-propagating long waves, amplitude-modulated wave packet, and an oscillating tail. Five different cases with different Δ were introduced to assess the sensitivity of the energy transfer process to the Δ. From the comparison between different cases, we have found the amplitude-modulated wave packets were the most sensitive to the Δ, followed by the oscillating tails, while the forward-propagating long waves were robust to different Δ. The amplitude-modulated wave packet was suggested playing an important role in energy transfer process during the early stage of modulation. The energy analysis of case 1 demonstrated in the first 30 periods, ~36% of the total energy of the mode-2 ISW was lost at an average rate of 9 W m^{-1}, which would deplete the energy of mode-2 ISW in ~4.5 h, corresponding to a propagation distance of ~5 km. Thus, we concluded the mode-2 ISWs are ephemeral in the presence of shear currents, and it was consistent with the hypothesis given by Shroyer et al. (2010). The ISW energy loss rates were found to decrease monotonically as the Δ increased which mean those wave forms shed from the

mode-2 ISW were more energetic in small Δ cases. In future work, a detailed investigation of generation mechanisms of different wave forms shed from the mode-2 ISW are needed to explain the divergence in their sensitivity to the Δ.

References

Akylas, T. R., & Grimshaw, R. H. J. Solitary internal waves with oscillatory tails. J.Fluid Mech, 242, 279-298, 1992.

Apel, J. R., Holbrook, J. R., Liu, A. K., & Tsai, J. J.. The sulu sea internal soliton experiment. J.phys.oceanogr, 15(12), 1625-1651, 1985.

Brandt, A., & Shipley, K. R. Laboratory experiments on mass transport by large amplitude mode-2 internal solitary waves. Phys.Fluids, 26(4), 016602-82, 2014.

Carr, M., Davies, P. A., &Hoebers, R. P. Experiments on the structure and stability of mode-2 internal solitary-like waves propagating on an offset pycnocline. Phys.Fluids, 27(4), 046602, 2015.

Carr, M., Fructus, D., Grue, J., Jensen, A., & Davies, P. A. Convectively induced shear instability in large amplitude internal solitary waves. Phys. Fluids, 20(12), 126601, 2008.

Chen, G. Y., Liu, C. T., Wang, Y. H., & Hsu, M. K. Interaction and generation of long‐crested internal solitary waves in the South China Sea. J.Geophys.Res., 116(C6), 1-7, doi:10.1029/ 2010JC006392, 2011.

Clarke, S., Grimshaw, R., Miller, P., Pelinovsky, E., & Talipova, T. On the generation of solitons and breathers in the modified Korteweg–de Vries equation. *Chaos:* An Interdisciplinary Journal of Nonlinear Science, 10(2), 383-392, 2000.

Colosi, J. A., Beardsley, R. C., Lynch, J. F., Gawarkiewicz, G., Chiu, C. S., &Scotti, A. Observations of nonlinear internal waves on the outer new England continental shelf during the summer shelf break primer study. J.Geophys.Res., 106(C5), 9587–9601, 2001.

Deepwell, D., &Stastna, M. Mass transport by mode-2 internal solitary-like waves. Phys.Fluids,28(5), 395-425, 2016.

Farmer, D., Li, Q., & Park, J. H. Internal wave observations in the South China Sea: The role of rotation and non‐linearity. Atmosphere-Ocean, 47(4), 267-280, 2009.

Fringer, O. B., & Street, R. L. The dynamics of breaking progressive interfacial waves. J.Fluid Mech.,

494, 319-353, 2003.

Grimshaw, R., Pelinovsky, E., Talipova, T., & Kurkina, O. Internal solitary waves: propagation, deformation and disintegration. Nonlinear Processes in Geophys., 17(6), 633, 2010.

Helfrich, K. R., & Melville, W. K. On long nonlinear internal waves over slope-shelf topography. J.Fluid Mech.,167(167), 285-308, 1986.

Helfrich, K. R., & Melville, W. K. Long nonlinear internal waves. Annu. Rev. Fluid Mech., 38, 395-425, 2006.

Helfrich, K. R., & White, B. L. A model for large-amplitude internal solitary waves with trapped cores. Nonlinear Processes in Geophys., 17(4), 303-318, 2010.

Hüttemann, H., &Hutter, K. Baroclinic solitary water waves in a two-layer fluid system with diffusive interface. Exp.Fluids,30(3), 317-326, 2001.

Klymak, J. M., & Moum, J. N. Internal solitary waves of elevation advancing on a shoaling shelf. Geophys.Res.Lett., 30(20), 2003.

Klymak, J. M., Pinkel, R., Liu, C., Liu, A. K., & David, L.Prototypical solitons in the South China Sea. Geophys.Res.Lett., 33(11), 2006.

Lamb, K. G. Internal wave breaking and dissipation mechanisms on the continental slope/shelf. Ann. Rev. Fluid Mech., 46, 231-254, 2014.

Lamb, K. G., & Farmer, D. (2011). Instabilities in an internal solitary-like wave on the oregon shelf. J.Phys.Oceanogr., 41(1), 67-87, 2011.

Lamb, K. G., & Nguyen, V. T. Calculating energy flux in internal solitary waves with an application to reflectance. J.Phys.Oceanogr., 39(3), 559-580, 2009.

Lamb, K. G., Polukhina, O. E., Talipova, T., Pelinovsky, E., Xiao, W., & Kurkin, A. Breather generation in fully nonlinear models of a stratified fluid. Phys.Rev.E, 75(4), 2007.

Legg, S., & Adcroft, A. Internal wave breaking at concave and convex continental slopes. J.Phys.Oceanogr, 33(11), 2224-2246, 2003.

Legg, S., & Huijts, K. M. Preliminary simulations of internal waves and mixing generated by finite amplitude tidal flow over isolated topography. Deep Sea Research Part II: Topical Studies in Oceanography, 53(1), 140-156, 2006.

Legg, S., & Klymak, J. (2008). Internal hydraulic jumps and overturning generated by tidal flow over a tall steep ridge. J.Phys.Oceanogr, 38(9), 1949-1964, 2008.

Liu, A. K., Chang, Y. S., Hsu, M. K., & Liang, N. K. Evolution of nonlinear internal waves in the East and South China Seas. J.Geophys.Res, 103(C4), 7995-8008, 1998.

Liu, A. K., Ramp, S. R., Zhao, Y., & Tang, T. Y. A case study of internal solitary wave propagation during ASIAEX 2001. IEEE J.Oceanic Eng., 29(4), 1144-1156, 2004.

Liu, A. K., Su, F. C., Hsu, M. K., Kuo, N. J., & Ho, C. R. Generation and evolution of mode-two internal waves in the South China Sea. Cont.Shelf Res., 59, 18-27, 2013.

Marshall, J., Hill, C., Perelman, L. T., &Adcroft, A. Hydrostatic, quasi-hydrostatic, and nonhydrostatic ocean modeling. J.Geophys.Res., 5733-5752, 1997.

Moum, J. N., Klymak, J. M., Nash, J. D., Perlin, A., & Smyth, W. D.Energy transport by nonlinear internal waves. J.Phys.Oceanogr.,37(7), 1968-1988, 2006.

Olsthoorn, J., Baglaenko, A., &Stastna, M. Analysis of asymmetries in propagating mode-2 waves. Nonlinear Processes in Geophys.,20(1), 59-69, 2013.

Orr, M. H., & Evans, T. E. Mode 2 Internal Wave Generation and Propagation Near the New Jersey (USA) Shelf Break-Early Fall Season (No. NRL/MR/7100--15-9602). Naval Rresearch Lab Washington DC, 2015.

Ostrovsky, L. A., &Stepanyants, Y. A. Do internal solitons exist in the ocean? revgeophys. Rev.Geophys., 27(3), 293–310, 1989.

Pawlak, G., & Armi, L. Vortex dynamics in a spatially accelerating shear layer. J.Fluid Mech., 376, 1-35, 1998.

Ramp, S. R., Yang, Y. J., Reeder, D. B., & Bahr, F. L. Observations of a mode-2 nonlinear internal wave on the northern heng-chun ridge south of taiwan. J.*Geophys.Res.,117(C*3), 3043, 2012.

Salloum, M., Knio, O. M., & Brandt, A. Numerical simulation of mass transport in internal solitary waves.Phys.Fluids,24(24), 21-110, 2012.

Shroyer, E. L., Moum, J. N., & Nash, J. D. Mode 2 waves on the continental shelf: ephemeral components of the nonlinear internal wavefield. J.Geophys. Res.,115(C7), 419-428, 2010.

Stastna, M., &Peltier, W. R. On the resonant generation of large-amplitude internal solitary and solitary-like waves. J.Fluid Mech.,543(543), 267-292, 2005.

Stastna, M., Olsthoorn, J., Baglaenko, A., &Coutino, A. Strong mode-mode interactions in internal solitary-like waves. Phys.Fluids,27(4), 046604, 2015.

Sutherland, B. R., Barrett, K. J., & Ivey, G. N. Shoaling internal solitary waves. J.Geophys.Res., 118(9),

4111-4124, 2013.

Talipova, T. G., Pelinovsky, E. N., &Kharif, C. Modulation instability of long internal waves with moderate amplitudes in a stratified horizontally inhomogeneous ocean. JETP Lett.,94(3), 182-186, 2011.

5   Terletska, K., Jung, K. T., Talipova, T., Maderich, V., Brovchenko, I., &Grimshaw, R. Internal breather-like wave generation by the second mode solitary wave interaction with a step. Phys.Fluids, 28(11), L03601-276, 2016.

Venayagamoorthy, S. K., & Fringer, O. B. On the formation and propagation of nonlinear internal boluses across a shelf break. J. Fluid Mech., 577, 137-159, 2007.

10   Vlasenko, V. I. Generation of second mode solitary waves by the interaction of a first mode soliton with a sill. Nonlinear Processes in Geophys.,8(4/5), 223-239, 2001.

Vlasenko, V., & Stashchuk, N.. Internal tides near the Celtic Sea shelf break: A new look at a well known problem. Deep Sea Research Part I: Oceanographic Research Papers, 103, 24-36, 2015.

Vlasenko, V., Stashchuk, N., Guo, C, & Chen, X. Multimodal structure of baroclinic tides in the South

15   China Sea. Nonlin. Processes in Geophys., 17(5), 529, 2010.

Wang, J., R. G. Ingram, and L. A. Mysak, Variability of internal tides in the Laurentian Channel. J. Geophys. Res., 96(C9), 16859–16875, doi:10.1029/91JC01580, 1991

Xu Z. H., B Yin, Y Hou, and Y Xu. Variability of internal tides and near-inertial waves on the continental slope of the northwestern South China Sea. J. Geophys. Res. Oceans, 118(1), 197–

20   211, doi:10.1029/2012JC008212, 2013

Xu Z. H., K Liu, B Yin, Z Zhao, Y Wang, and Q Li. Long-range propagation and associated variability of internal tides in the South China Sea. J. Geophys. Res. Oceans, 121(11), 8268–8286, doi:10.1002/2016JC012105, 2016

Yang, Y. J., Fang, Y. C., Chang, M. H., Ramp, S. R., Kao, C. C., & Tang, T. Y. Observations of second

25   baroclinic mode internal solitary waves on the continental slope of the northern south china sea. J.Geophys.Res.,114(C10), 637-644, 2009.

Yang, Y. J., Fang, Y. C., Tang, T. Y., & Ramp, S. R. Convex and concave types of second baroclinic mode internal solitary waves. Nonlinear Processes in Geophys.,17(6), 605-614, 2010.

Yuan, C., Grimshaw, R., & Johnson, E. The evolution of second mode internal solitary waves over

30   variable topography. J.Fluid Mech., 836, 238-259, 2018.

Zhao, Z., Klemas, V., Zheng, Q., & Yan, X. Remote sensing evidence for baroclinic tide origin of internal solitary waves in the northeastern south china sea. Geophys.Res.Lett., 31(6), L06302, 2004.

Zhao, Z., & Alford, M. H. Source and propagation of internal solitary waves in the northeastern south
5   china sea. J.Geophys.Res., 111(C11), 63-79, 2006.